88. K. D. Caldwell, Z.-Q. Cheng, P. Hradecky, J. C. Giddings, *Cell Biophys.* **6**, 233 (1984).
89. P. J. P. Cardot, J. Gerota, M. Martin, *J. Chromatogr.* **568**, 93 (1991).
90. A. Merino-Dugay, P. J. P. Cardot, M. Czok, M. Guernet, A. P. Andreux, *ibid.* **579**, 73 (1992).
91. A. Merino, C. Bories, J.-C. Gantier, P. J. P. Cardot, *ibid.* **572**, 291 (1991).
92. J. C. Bigelow, Y. Nabeshima, K. Kataoka, J. C. Giddings, *ACS Symp. Ser.* **464**, 146 (1991).
93. B. N. Barman, E. R. Ashwood, J. C. Giddings, *Anal. Biochem.*, in press.
94. S. Hoffstetter-Kuhn, T. Rösler, M. Ehrat, H. M. Widmer, *ibid.* **206**, 300 (1992).
95. J. C. Giddings, M. N. Myers, M. H. Moon, B. N. Barman, *ACS Symp. Ser.* **472**, 198 (1991).
96. M. H. Moon and J. C. Giddings, *Anal. Chem.* **64**, 3029 (1992).
97. J. C. Giddings, S. K. Ratanathanawongs, M. H. Moon, *KONA: Powder Particle* **9**, 200 (1991).
98. B. N. Barman, M. N. Myers, J. C. Giddings, *Powder Technol.* **59**, 53 (1989).
99. P. M. Shiundu, E. E. Remsen, J. C. Giddings, unpublished results.
100. M. A. Benincasa and J. C. Giddings, *Anal. Chem.* **64**, 790 (1992).
101. P. Sinclair, R. Beckett, B. T. Hart, *Hydrobiologia* **176/177**, 239 (1989).
102. R. Beckett and B. T. Hart, in *Environmental Particles*, J. Buffle and H. P. Van Leeuwen, Eds. (CRC Press, Boca Raton, FL, 1993), vol. 2, pp. 157–195.
103. G. Karaiskakis, K. A. Graff, K. D. Caldwell, J. C. Giddings, *Int. J. Environ. Anal. Chem.* **12**, 1 (1982).
104. R. Beckett, G. Nicholson, B. T. Hart, M. Hansen, J. C. Giddings, *Water Res.* **22**, 1535 (1988).
105. H. E. Taylor, J. R. Garbarino, D. M. Murphy, R. Beckett, *Anal. Chem.* **64**, 2035 (1992).
106. R. Beckett, D. M. Hotchin, B. T. Hart, *J. Chromatogr.* **517**, 435 (1990).
107. J. F. McCarthy, J. M. Zachara, *Environ. Sci. Technol.* **23**, 495 (1989).
108. D. J. Chittleborough, D. M. Hotchin, R. Beckett, *Soil Sci.* **153**, 341 (1992).
109. R. Beckett, Z. Jue, J. C. Giddings, *Environ. Sci. Technol.* **21**, 289 (1987).
110. R. Beckett, J. C. Bigelow, J. Zhang, J. C. Giddings, *Adv. Chem. Ser.* **219**, 65 (1989).
111. R. Beckett, F. J. Wood, D. R. Dixon, *Environ. Technol.*, in press.
112. R. V. Sharma, R. T. Edwards, R. Beckett, *Appl. Environ. Microbiol.*, in press.
113. This work was supported by grant CHE-9102321 from the National Science Foundation and Public Health Service grant GM10851-36 from the National Institutes of Health.

High-Resolution and Analytical Transmission Electron Microscopy of Mineral Disorder and Reactions

David R. Veblen, Jillian F. Banfield, George D. Guthrie, Jr.,
Peter J. Heaney, Eugene S. Ilton, Kenneth J. T. Livi,
Eugene A. Smelik

Crystal defects and chemical reactions occurring at scales beyond the resolution of light microscopes have major effects on the chemical and physical properties of rocks and minerals. High-resolution imaging, diffraction, and chemical analysis in the transmission electron microscope have become important methods for exploring mineral defect structures and reaction mechanisms and for studying the distribution of phases resulting from reactions. These techniques have shown that structural disorder is common in some rock-forming minerals but rare in others. They have also established mechanisms by which many reactions occur at the atomic cluster scale. These data thus provide an atomistic basis for understanding the kinetics of geological reactions. Furthermore, apparent major-element, minor-element, and trace-element chemistry of minerals can be influenced by submicroscopic inclusions or intergrowths, which commonly form as products of solid-state reactions.

Transmission electron microscopy (TEM) has long been an important experimental technology in materials science, solid-state physics, and solid-state chemistry. Most processes of interest in these fields have analogs in the geological sciences, although the terminology used to describe them may differ. For example, materials scientists refer to degradation of metals as corrosion, whereas geochemists refer to mineral degradation occurring at Earth's surface as weathering. Annealing of metals is similar in many ways to contact metamorphism, and deformation of materials and rocks proceeds by the same mechanisms, although commonly at much different spatial and time scales. Indeed, much has been learned about the behavior of geological materials from experiments on metals, which typically exhibit much faster diffusion rates and deform plastically at much higher strain rates than most minerals.

Much can also be learned about solid-state materials from processes observed in minerals. Many rock-forming silicates have complex structures with relatively low symmetry (triclinic, monoclinic, or orthorhombic) and thus can provide an understanding of phase transformations in low-symmetry materials of technological interest. Although diffusion is sluggish in most silicates (zeolites and some clays excepted), geological time is immense compared with laboratory time scales, making minerals good analogs for materials processed for long periods. Among the thousands of mineral species are found the archetypes for many of our technologically vital materials. For example, the uncommon mineral perovskite ($CaTiO_3$) lends its name to the silicate perovskite structures such as high-pressure $MgSiO_3$, which are probably the most abundant minerals in the Earth's interior, as well as to numerous catalysts and ferroelectric materials, such as $BaTiO_3$. The perovskite structure is also the basis for many of the high-temperature superconductor structures, and the interest in structural variants, defects, and reactions in perovskite-based materials (*1*, *2*) spans the earth and materials science communities.

Just as TEM has revolutionized our understanding of the behavior of synthetic materials, these experimental tools are also being applied to the chemically complicated materials important in the earth sciences. Since the development of the quantitative analysis of fault displacements in the 1950s (*3*), conventional amplitude-contrast electron microscopy has made many fundamental contributions in the understanding of deformation mechanisms, in determining the textural relations between phase distributions, and in understanding processing conditions in metals and ceramics. By the mid-1970s geologists were routinely applying electron diffraction and conventional electron microscopy to similar problems in minerals (*4*). Indeed, amplitude-contrast imaging remains the primary method for examining both dislocations produced by deformation (*5*) and domain structures formed during phase transitions in minerals (*6*).

Great strides have been made during the past two decades in the development of TEM methods, including high-resolution TEM (HRTEM) and allied techniques, such as x-ray emission analytical transmission electron microscopy (AEM) (*7*) and convergent beam electron diffraction (CBED) (*8*). Furthermore, theoretical advances now make quantitative interpretation of results possible (*9*). Because these techniques are combined in many modern transmission electron micro-

---

D. R. Veblen and K. J. T. Livi are in the Department of Earth and Planetary Sciences, Johns Hopkins University, Baltimore, MD 21218. J. F. Banfield is in the Department of Geology and Geophysics, University of Wisconsin, Madison, WI 53706. G. D. Guthrie, Jr., is in the Earth and Environmental Sciences Division, Los Alamos National Laboratory, Los Alamos, NM 87545. P. J. Heaney and E. A. Smelik are in the Department of Geological and Geophysical Sciences, Princeton University, Princeton, NJ 08544. E. S. Ilton is in the Department of Geological and Environmental Sciences, Lehigh University, Bethlehem, PA 18015.

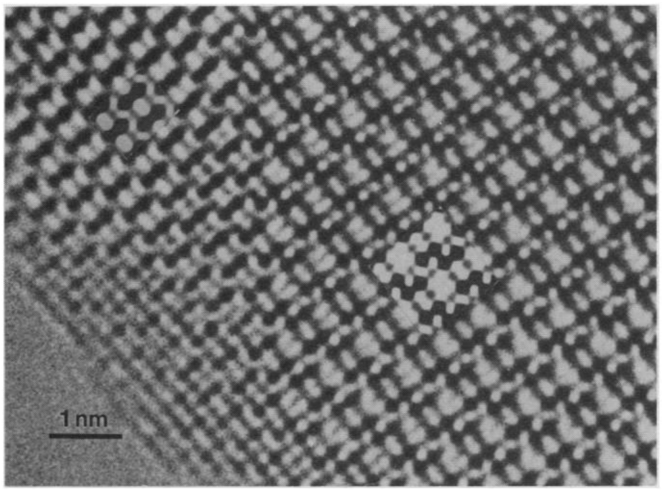

Fig. 1. HRTEM image (Scherzer focus) from a wedge-shaped specimen containing the interface between anatase (left) and a new TiO_2 mineral (*14*). Simulated images are inset for both phases. Image contrast changes as the crystal thickens to the upper right. [Modified from (*14*)]

scopes, they can yield both fine-scale chemical and structural data, which make these instruments useful to many Earth science disciplines, from high-pressure mineral physics to low-temperature geochemistry. Furthermore, these TEM methods potentially can be combined with other approaches, such as x-ray diffraction, electron microprobe chemical analysis, various types of vibrational and nuclear magnetic resonance spectroscopy (*10*, *11*), surface analysis using Auger electron and x-ray photoelectron spectroscopies (*12*), and surface imaging achieved with the scanning-probe microscopies (*13*), to characterize a solid in unprecedented detail. In this article we concentrate, through selected examples from our work, on data about structure and chemical reactions that are acquired in HRTEM and AEM studies of minerals. These examples illustrate the complex reaction behavior that is typical of structurally complicated, low-symmetry materials. However, electron microscopic methods produce even greater results if they are combined with other techniques, such as surface analysis.

Chemical and mineral distributions resulting from reactions provide much useful information regarding petrogenesis and the development of complex textures in solid materials in general. The temperature and pressure histories of igneous and metamorphic rocks typically are deduced from analyses of the phase assemblages and the compositions of coexisting minerals, which result directly from heterogeneous and exchange reactions (*14*). The rates of some processes can be estimated from the stranded states resulting from sluggish reaction kinetics, such as chemical zoning profiles in mineral crystals (*15*). Similarly, the physical properties of many rocks are related to their reaction histories and the defect structures of their constituent minerals. Magnetic properties are controlled in part by the reactions that produce magnetic minerals, and the gross structure of the Earth reflects in large part mineral transformations and the resulting density variations that occur within it. Finally, environmental processes, such as the mobilization (or stabilization) of toxic metals, are controlled largely by the interactions of aqueous fluids with soil minerals.

Phase transformations can drastically affect material properties. Mechanical properties in alloys, for example, can be engineered by processes such as precipitation hardening. The structural and electronic changes occurring at higher order phase transitions are key for understanding the bulk behavior of materials from piezoelectrics to superconductors. Reactions and phase transitions in minerals are studied over an even greater range of scales. For example, seismic tomography has been used to map vertical and horizontal density variations, which indicate gross changes in chemistry and crystal structure within the Earth. In contrast, traditional geochemical techniques, such as bulk chemical analysis and optical microscopy, provide compositional and textural information at macroscopic scales on the order of tens of micrometers to centimeters. Both experimental and observational petrology were revolutionized by the electron microprobe, which permitted accurate chemical analyses of coexisting minerals and inhomogeneities in minerals at the micrometer scale. Imaging resolutions in the TEM are now routinely well below 1 nm (*9*) and analytical spatial resolutions approach 10 nm (*7*).

Characterization of Minerals and Extended Defects

Modern TEM methods allow determination of chemical composition, unit-cell parameters, symmetry, and in some cases even the crystal structure of extremely small sample areas. Similarly, it is possible to explore nonperiodic structural aspects of minerals, such as extended defects, at high resolutions. Because these features are often produced by crystallization or postcrystallization processes, they may serve as a record of the physical and chemical history of the specimen.

A study of a recently discovered titanium dioxide mineral serves to illustrate several capabilities of the modern TEM (*16*). The new mineral was first observed as narrow, submicrometer lamellae in anatase, a low-temperature TiO_2 polymorph known for its catalytic properties, from Vallais Bintal, Switzerland. AEM analyses of the lamellae were identical to those from adjoining anatase, but selected area electron diffraction and CBED patterns could not be indexed to any of the known TiO_2 minerals. It thus appeared that the lamellae represented a new TiO_2 mineral. In order to determine a model for its structure, HRTEM images were acquired with the use of a 400-keV instrument with a point-to-point resolution of 0.17 nm (*16*).

High-resolution images obtained from thin regions of the specimen at the Scherzer focus (sometimes called the optimum defocus) consisted of a periodic array of black spots (Fig. 1). The black spots apparently correspond to columns of Ti atoms that are in octahedral (sixfold) coordination with oxygen. Computer simulations for such a model closely resembled the experimental images obtained in two orientations, not only at the Scherzer focus (Fig. 1) but over a range of defocus values.

The agreement between experimental and simulated HRTEM images suggests that the structural model for this new mineral is correct. Indeed, the determined structure is identical to that reported previously for the metastable phase TiO_2 (B), a synthetic catalyst material (*17*) previously unknown in nature. The above example is but one of several approaches to structure determination currently being explored by electron microscopists. Other methods with great potential include direct measurement of structure factors with CBED (*8*) and determination of diffraction phases from HRTEM images of extremely thin crystals (*18*). An important difference between standard diffraction methods using x-rays or neutrons is that electron microscopy methods of structure determination may be applicable to isolated defects, whereas normal structure determination and refinement methods are applicable only to average crystal structures.

Replacement Reactions

There commonly are several different routes for the synthesis of materials. Similarly, many different types of mineral-forming reactions occur within Earth's interior and at the surface. Minerals can nucleate and crystallize directly from silicate melts, from

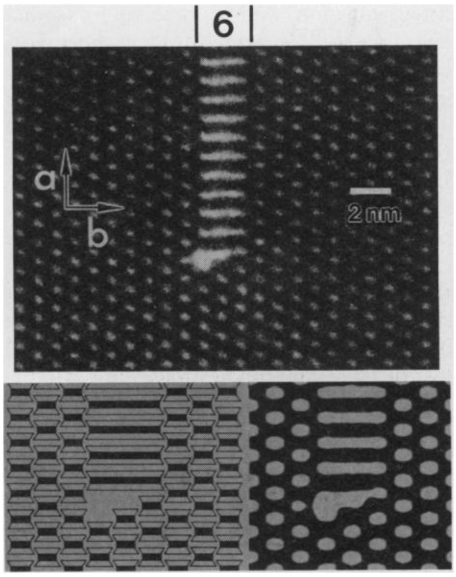

Fig. 2. HRTEM image of a terminating slab of sextuple-chain silicate in the double-chain silicate anthophyllite (*23*). Such defects can form during reactions, and in this case the wide-chain structure is replacing the anthophyllite by growth of the defect at its termination. The model structure (lower left) is shown using large structural blocks rather than individual atoms, and the computer simulation (lower right) was derived from this model. [Modified from (*23*)]

hot fluids in hydrothermal systems, and from sea water to produce chemical sediments, such as limestone. Especially at low temperatures, growth directly from a fluid often produces highly defective crystals, and electron microscopy has effectively characterized growth defects in numerous minerals, for example, in micas and carbonates (*19*). Reactions in preexisting rocks, however, have been studied more extensively. Such reactions occur during processes from diagenesis to mantle phase transitions, and they are analogous to many reactions produced during annealing in metals and ceramics. Just as in synthetic materials (*20*), defect distributions in minerals depend on the mechanism and conditions of formation or alteration.

A mineral or an assemblage of minerals is usually replaced by another phase assemblage in one of two ways. Existing minerals may dissolve at the surface, with essential components transported along the grain boundaries. New minerals then may precipitate between existing grains (*21*). Alternatively, minerals or mineral assemblages can be replaced directly by solid-state reactions. In such reactions, the crystal structures of the reactant and product commonly are finely intergrown or in intimate contact during the reaction (*22*). The phases are commonly oriented with respect to each other, in which case the reaction may be called topotactic. Reaction products that minimize interfacial energy with the reactant structure may be favored, compared with the thermodynamically stable phase, leading in some cases to metastable reaction paths. Most important for the study of such reactions with electron microscopy are the microstructures and chemical distributions in incompletely reacted samples, from which structural reaction mechanisms may be inferred.

Reactions involving the transformation of chain silicates to sheet silicates are often topotactic. For example, Fig. 2 (*23*) shows a lamella of sextuple-chain silicate that has partially replaced the double-chain amphibole structure. Such zippers typically nucleate at or near grain boundaries or fractures and advance into the interior of the crystal by consuming the reactant. HRTEM images may be used to infer mass balance. For example, the reaction illustrated structurally in Fig. 2 may be expressed chemically as

$$\underset{\text{amphibole}}{3(\mathrm{Mg,Fe})_7\mathrm{Si}_8\mathrm{O}_{22}(\mathrm{OH})_2 + 4\mathrm{H}^+} \rightarrow$$

$$\underset{\text{sextuple-chain silicate}}{(\mathrm{Mg,Fe})_{19}\mathrm{Si}_{24}\mathrm{O}_{62}(\mathrm{OH})_{10} + 2(\mathrm{Mg,Fe})^{2+}}$$

The sextuple-chain silicate formed in this arrested reaction is an intermediate product in the reaction of amphibole to the sheet silicate talc. Sextuple-chain silicate is not a stable phase in the MgO-FeO-$\mathrm{SiO_2}$-$\mathrm{H_2O}$ system, and therefore it represents a metastable intermediate structure that is kinetically favored to form because of its low-strain-energy match with the parent amphibole structure.

The above reaction indicates that hydrogen in some form must diffuse into the parent structure, and Mg and Fe must diffuse out of the crystal. The single-chain silicates called pyroxenes commonly exhibit similar reaction-induced defect structures, but diffusion coefficients measured in pyroxenes (*24*) suggest that bulk (or lattice) diffusion through the structure is too sluggish to account for analogous reactions in single-chain silicates (*25*). Thus, most of the chemical transport necessary for such reactions likely occurs along the structurally disrupted zones at the terminations of advancing lamellae, similar to the one shown in Fig. 2. Calculated images imply that these zones are linear tunnels with cross sections similar to the pore diameters of many zeolite structures, in which diffusion is many orders of magnitude more rapid than in chain silicates. Where diffusion is the rate-controlling step in the reaction, linear defects of this type may constrain solid-state reaction kinetics. Analogous disrupted zones occur at lamellar terminations in many rock-forming minerals, such as in partially reacted pyroxenes, amphiboles, pyroxenoids, sheet silicates such as micas and chlorite, and olivine (*25, 26*). All of these possess structures that can be interpreted as being constructed from layer modules. It is likely that reactions in synthetic materials with analogous structures, such as the layered high-temperature superconductors (*2*) and metal oxides based on the $\mathrm{ReO_3}$ structure type (*27*), involve similar fast diffusion at the terminations of growing defects. However, precise atomistic diffusion paths, for example in reduction reactions of $\mathrm{WO_3}$, have yet to be experimentally determined (*28*).

In some cases, replacement reactions do not occur by the propagation of isolated and narrow lamellae but by the advancement of a two-dimensional reaction front, which can be described as a grain boundary between oriented reactant and product. In such cases, the structure of the reaction front may consist of a periodic array of line defects, similar to those that occur at the reaction site for the lamellar reaction mechanism. Thus, much of the diffusion necessary for the reaction probably occurs along analogous channels that are now organized into a grain boundary.

Exsolution

Exsolution, or precipitation, reactions occur when an initially homogeneous material becomes unstable and separates into two or more immiscible phases. Such reactions are crucial for the mechanical properties of many alloys (*29*) and glass-ceramics (*30*). Analogous reactions in rock-forming minerals occur in the solid state and commonly take place during the slow cooling of feldspars and chain silicates from their temperatures of formation. A miscibility gap (for example, a solvus) allows phase separation to take place either by nucleation and growth or by a continuous spinodal decomposition mechanism.

A major use of TEM methods is to characterize exsolution textures, which can be used to infer the processes that produced the phase-separated texture. Such studies of alloys and ceramics are important for optimization of synthesis and processing conditions. In minerals, exsolution textures and chemistry also may be used to infer extensive variables (temperature, pressure, chemical activities) and cooling rates at the time of exsolution. There have been numerous studies of exsolution relations between Ca-rich and Ca-poor pyroxenes (*31*), as well as immiscibility in both the alkali and plagioclase feldspar (framework silicate) systems (*32, 33*). An example that illustrates a complex interface structure resulting from exsolution in low-symmetry minerals is shown in Fig. 3 (*34*). The interface is between host augite (high-Ca monoclinic pyroxene) and a lamella of pigeonite (low-Ca monoclinic pyroxene), which has precipitated from the initially homogeneous pyroxene crystal that formed at higher temperatures. As interpreted from conventional, amplitude-contrast TEM experiments (*35*), this type of complicated boundary formed from a sequence of events. First, the pigeonite lamella nucleated at temperatures between 800° and 1000°C from the host augite. The boundary initially was coherent (it contained no dislocations), and dimensional misfit between the augite (Ca-rich) and pigeonite (Ca-poor) lattices was accommodated in two ways: (i) the interface adopted an irrational orientation close to (001) and (ii) the (100) planes of the pigeonite lattice rotated with respect to those of the augite lattice. As cooling proceeded, however, the unit-cell dimensions of the pigeonite and augite changed unequally, and major changes occurred near a phase transition at approximately 725°C. At this temperature, the pigeonite lamella inverted from a C-centered monoclinic structure to a primitive monoclinic structure. Because of strain from the considerable changes in lattice parameters, the initial interface orientation destabilized. Formation and movement of partial dislocations reduced strain by producing stacking faults in the pigeonite lamella, and additional strain was accommodated by further rotations of the pigeonite lattice. The present lattice rotation can be seen by viewing the image (Fig. 3) at a low angle along the lattice fringes that are nearly vertical. Each dislocation is dissociated into two equal partial dislocations to create a final interface with a curious stepped morphology (Fig. 3). This interface is considerably more complicated than typical precipitation-produced interfaces in metals and simple ceramics, owing in part to the more complex crystal structures and lower symmetry of these silicates. Feldspars (*33*) and other low-symmetry minerals can also display a wide array of complex exsolution textures. As materials with increasingly more complex chemistry and structure are examined (for example, oxide superconductors), similar complicated interfaces produced by precipitation may be found to be common, especially in relatively low symmetry materials.

In contrast to pyroxenes, most amphiboles do not have exsolution textures that are resolvable with a light microscope, although some slowly cooled metamorphic amphiboles show fine-scale lamellae of a second amphibole (*36*). Recent TEM studies of submicroscopic (invisible to light microscopes) exsolution in amphiboles have identified calcic amphibole (hornblende) exsolved from the orthorhombic amphibole gedrite (*37*) and exsolution within the calcic amphibole series actinolite-hornblende and in the orthoamphibole series anthophyllite-gedrite (*38*). Exsolution has also been seen with analytical electron microscopy in Mn-rich alkali amphiboles (*39*). No apparent exsolution visible with light occurs in glaucophane, a sodic amphibole (*40*) that is abundant in high-pressure, subduction-zone metamorphism. TEM studies showed, however, that glaucophane may have exsolution textures, including lamellae of ferromagnesian, calcic, and sodic-calcic amphibole (*41*).

A particularly complex exsolution texture occurs in glaucophane from high-pressure rocks in northern Vermont, which are apparently remnants from a subduction-zone metamorphic episode related to the closing of the Proto-Atlantic Ocean early in the Paleozoic Era (*42*). As shown by Figs. 4 and 5, which illustrate the capability of obtaining high-resolution chemical, textural, and crystallographic information (*43*), there were several phase separation events. Based on textural relations and x-ray emission AEM, lamellae of sodic-calcic amphibole (winchite) first precipitated approximately parallel to (100) of the glaucophane host, followed by exsolution of a metastable ferromagnesian amphibole (cummingtonite) with unusually high Ca. In places, the high-Ca cummingtonite further exsolved to periodic lamellae of a normal, low-Ca cummingtonite and the calcic amphibole actinolite (Fig. 5). Thus, the initially homogeneous silicate now consists of a texturally complex mixture of five compositionally distinct amphiboles. All five of these amphiboles have similar unit-cell parameters, and, indeed, all have $C2/m$ space-group symmetry.

The above observations lead to several conclusions about exsolution in chemically complicated materials. Under slow cooling rates, exsolution can be a multistage process consisting of a sequence of metastable and stable steps. More than two mutually immis-

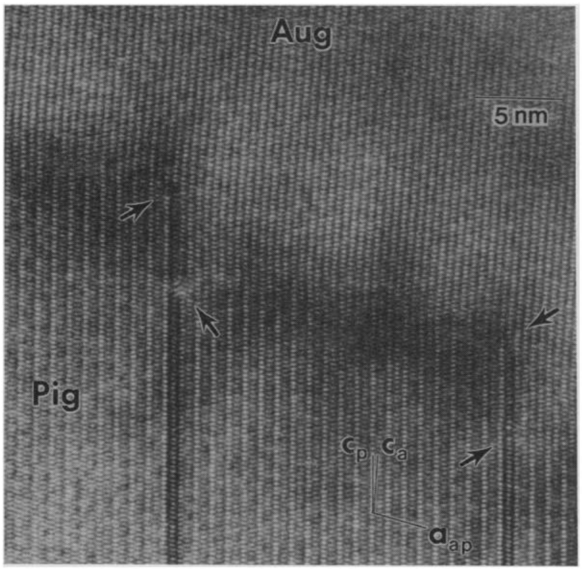

Fig. 3. A complex interface between host augite (Aug) and a lamella of pigeonite (Pig) that has precipitated from the augite during cooling from igneous temperatures (*34*). The augite and pigeonite lattices are rotated relative to each other. Interface dislocations are dissociated into partials (arrows), creating a stepped interface morphology. [Modified from (*34*)]

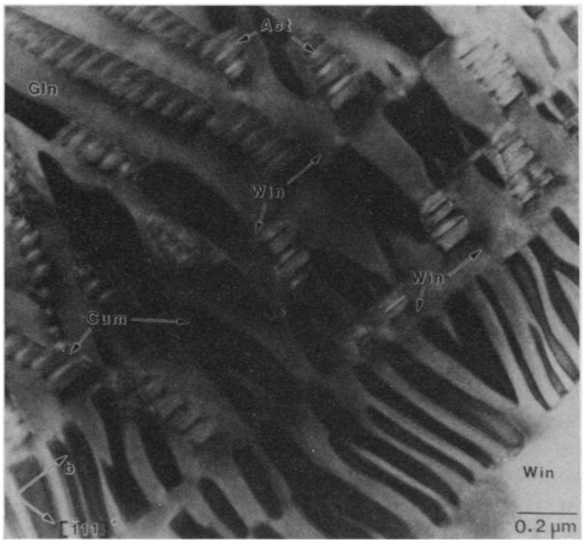

Fig. 4. An initially homogeneous, high-pressure amphibole crystal that decomposed into five compositionally distinct amphiboles: the glaucophane host and lamellae of winchite; metastable, high-Ca cummingtonite; normal, low-Ca cummingtonite; and actinolite. [Modified from (*43*)]

cible phases can precipitate out of a single solid solution, and, at low temperatures or with rapid cooling rates, complex textures may develop at scales well below the resolution of light microscopes. In synthetic materials, such submicroscopic textures can strongly affect mechanical properties, and it is likely that the rheological properties of rocks are similarly affected. Though well studied in structural materials, understanding the interactions between moving dislocations and other microstructures in rock-forming silicates remains one of the frontiers in the field of structural geology.

Fluid Inclusions

Aqueous fluids control many geological processes, such as deposition of ore minerals, formation and migration of petroleum, and explosive volcanism. The long-term storage of radioactive waste likewise depends on isolation from fluids that can corrode containers, dissolve waste, and transport radionuclides. As a result, one major challenge is to determine the chemistry, properties, and distribution of fluids in the Earth's crust. Whereas clues to temperature, pressure, and coexisting fluid chemistry sometimes can be found in the compositions of coexisting minerals, more direct information on the chemical compositions of geological fluids is contained in fluid inclusions in minerals and the daughter minerals that may crystallize from the inclusions. The study of relatively large fluid inclusions with Raman spectroscopy and light microscopes equipped with heating and cooling stages has produced important information about fluid compositions and the temperatures of formation or alteration of the surrounding minerals (*44*). The identification of daughter minerals is a critical step in evaluating the original fluid composition. In some cases, however, fluid inclusions are too small to examine by light optical methods, and here the imaging, diffraction, and analytical capabilities of the TEM may serve to identify the daughter minerals. For example, turbid diamonds and feldspars (*45–47*) are optically cloudy as a result of light scattering by submicrometer inclusions.

Ion microprobe and infrared spectroscopy studies of turbid diamonds revealed that the turbid regions contain small inclusions rich in K, Si, Ca, Fe, H_2O, and CO_3^{2-}, suggesting that the turbid parts of the diamond may have formed in the presence of a volatile-rich fluid in Earth's upper mantle (*45*). With the high spatial resolution of TEM methods, however, individual daughter crystals within the inclusions may be evaluated (Fig. 6) (*46*). Inclusions in turbid diamonds contain at least three families of daughter crystals: silicate, phosphate, and carbonate. Although the use of TEM in fluid inclusion research is in its infancy, major contributions can be expected in the analysis of small inclusions and submicroscopic daughter crystals.

In Situ Observations of Phase Transitions

Phase transitions in minerals and materials entail changes in symmetry but also commonly involve useful changes in physical properties. A magnetic material can be permanently magnetized below its Curie point. Similarly, a magnetic mineral acquires thermal remanent magnetism as it cools through this phase transition, providing the basis for paleomagnetic studies of igneous and metamorphic rocks. Other useful properties, such as piezoelectricity, are acquired at structural phase transitions in materials such as $BaTiO_3$ and quartz.

Electron microscopes may have a variety of sample stages to allow the specimen to be deformed, heated, or cooled or to come into contact with reactive gases (*48*). In situ TEM studies of minerals have lagged behind those for technologically important materials (*49*) but provide insights into transformation mechanisms in complex, low-symmetry structures. Examples of displacive phase transitions observed in minerals with heating stages include the formation of antiphase boundaries at the C-centered to primitive phase transition in the pyroxene pigeonite (*50*) and the formation of antiphase domains in the Ca feldspar anorthite (*51*).

The most intensively studied phase transition in a mineral is the α-β transition in the quartz polymorph of SiO_2 (*52*) because of the importance of quartz oscillators and other technological applications. Electron microscopy was key in the discovery of an incommensurate, modulated intermediate structure of quartz (*53*) that exists over a narrow temperature range of approximately 1.3°C between the low-temperature α phase (stable below approximately 573°C) and the high-temperature β phase. The intermediate phase was studied also by neutron diffraction (*54*), which showed that the modulation is not an artifact from surface effects in the thin specimen studied by electron microscopy. Similar intermediate modulated structures are also common at phase transitions in other materials, including $NaNO_2$ and $LiAlSiO_4$ (β-eucryptite) (*55*).

Among the phenomena associated with many structural phase transitions are hysteresis and memory effects (*56*). In calorimetry studies of quartz, for example, the temperature of transition from and to the α phase is offset by about 1° for the heating and cooling stages of a thermal cycle (*57*). In addition, when quartz is annealed within the stability field for the intermediate structure, the modulation wave vector and physical properties, such as birefringence, are observed to become pinned during subsequent thermal cycles at the values characteristic of the annealing temperature (*58*). These memory effects were attributed to the ordering of point defects into defect density waves (*59*).

Another memory effect is observed in the positions of the domain walls associated with Dauphiné twinning, which arises as a β

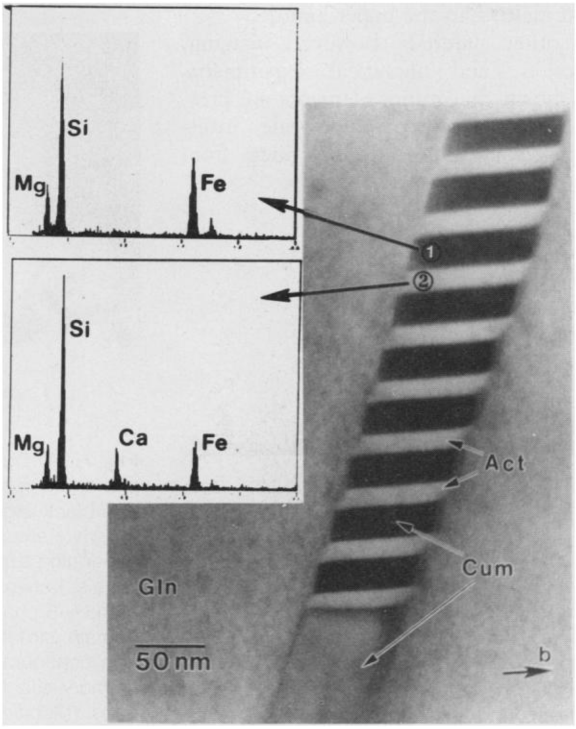

Fig. 5. A lamella of metastable, high-Ca cummingtonite in glaucophane. Part of the lamella has further decomposed, as shown by the x-ray emission spectra 1 (normal, low-Ca cummingtonite) and 2 (actinolite). [Modified from (*43*)]

quartz crystal is cooled through the transition temperature to α quartz (*60*). As shown in Fig. 7, quartz retains a memory of twins (the twin operation is a symmetry operation in the high-temperature phase) in the lower temperature phase after heating beyond the phase transition. In a kinetic study of this effect (*60*), quartz samples were thermally cycled from the α phase to the β phase, where they were held for a period and then cooled. Memory loss for each cycle was measured as the volume percentage that switched from one Dauphiné twin orientation to the other (that is, from white to black or from black to white). For a number of thermal cycles, the loss of memory increased with the amount of time the sample was held in the β field, and memory loss also increased with increases in the temperature of annealing. Such behavior is consistent with memory resulting from the pinning of domain walls by point defects.

After a quartz crystal was cycled through the transition region several times, however, memory improved. In crystals that were cycled many times, the memory for domain positions became nearly perfect, even for a sample annealed 300°C above the transition temperature. Such behavior is not consistent with simple point defect pinning of the domain walls. It is possible, however, that point defects controlling the positions of the domain walls eventually diffused to and remained in optimal positions or that point defects aggregated into relatively immobile clusters. Although this explanation is tentative, the behavior of the Dauphiné twin memory effect in quartz emphasizes the importance of defects and transformation-induced microstructures in the study of phase transitions.

Minor Elements

Impurity elements can detrimentally affect electronic properties in semiconductors and mechanical properties of alloys. On the other hand, intentional doping with desired impurities is essential in the fabrication of many semiconductor devices. In the geological sciences, trace and minor elements in minerals serve as chemical clues to the origin of rocks. A key question is whether levels of trace elements in minerals represent equilibrium partitioning between the solid and a fluid (for example, a silicate melt) or are determined kinetically by processes such as crystal growth. Other questions involve the role of crystal defects in controlling trace element incorporation in minerals (*61*) and the structural state of the trace element. For instance, are minor elements in true solid solution (involved in a homologous substitution within the basic structure of the mineral), or are they instead incorporated as submicroscopic inclusions of another phase?

The incorporation of potassium in high-pressure pyroxenes illustrates these issues. According to conventional wisdom, K cannot enter the pyroxene structure because of its large ionic radius (*62*), and the presence of K in reported pyroxene analyses results from inclusions, such as minute lamellae of intergrown amphibole. However, the combination of HRTEM and analytical electron microscopy demonstrated that measurable K can enter the structure; both x-ray emission analyses and images were obtained from exactly the same areas of a pyroxene (*63*). Apparently, up to 7% of the clinopyroxene M2 site can be occupied by K in regions that are completely free of extended defects or inclusions, an observation that may have implications for understanding the source of K in magma produced by partial melting in the upper mantle.

In other materials, however, imaging, diffraction, and analytical experiments have shown that minor elements are present predominantly in fine-scale intergrowths. For example, biotite micas from porphyry copper deposits commonly show anomalously high Cu contents in electron microprobe analyses (up to 13% of the oxide by weight, assuming the Cu to be present as CuO). Most workers have assumed that the Cu is dissolved homogeneously in the biotite crystal structure, suggesting that the Cu is introduced into the mica during magmatic crystallization or during the high-temperature hydrothermal alteration event in these deposits.

Imaging by TEM, electron diffraction, and AEM show conclusively, however, that anomalous Cu in natural biotite is present as inclusions of native (metallic) Cu, in inclusions of other minerals, such as the Fe oxyhydroxide goethite (FeOOH), or in intergrown vermiculite-like layers, as shown in Fig. 8A (*64*). These modes of occurrence suggest that the Cu is introduced at low temperatures and under oxidizing conditions, perhaps as a result of weathering reactions, instead of magmatic or hydrothermal temperatures.

To test this hypothesis, the micas biotite

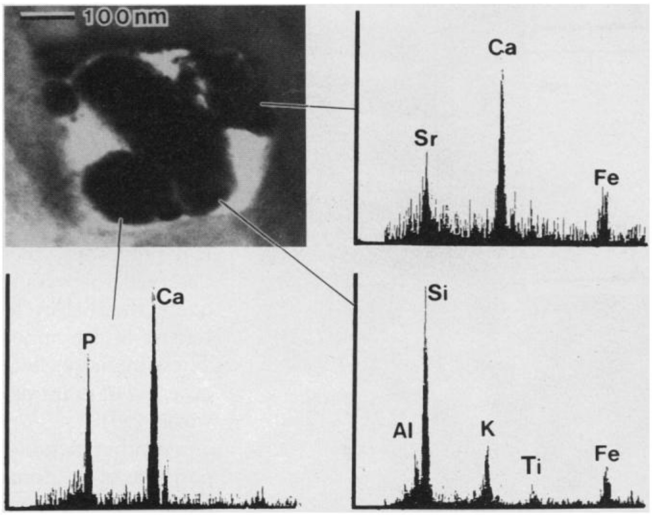

Fig. 6. A fluid inclusion in turbid diamond, which was ruptured during sample preparation by ion milling. X-ray emission analyses show that there are three chemically distinct daughter crystals in this single inclusion [Modified from (*46*)].

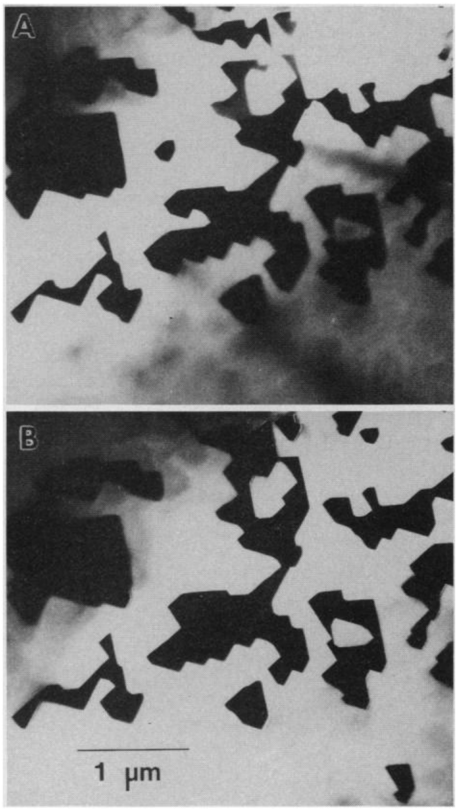

Fig. 7. (**A**) Dark-field image showing the Dauphiné twin configuration in a crystal of α quartz. The black areas are one twin orientation, and the white areas are the other, with domain walls separating the two. The crystal was heated in the electron microscope above the temperature of the α-β phase transition, thus destroying the domain structure. (**B**) Upon quenching, this twin configuration formed, indicating a strong memory effect for the positions of the domain walls. [Modified from (*60*)].

and phlogopite were experimentally reacted with $CuSO_4$ solutions at room temperature (65). Both micas reacted rapidly (on time scales of days); in some areas the Cu^{2+} was reduced, and many small metallic Cu crystals formed in the interlayer region of the mica (Fig. 8B). In other regions, Cu-rich, expanded, vermiculite-like interlayers formed, similar to those in Fig. 8A. The rapid rates of such reactions between silicates and metal-bearing fluids may have important implications for the migration and demobilization of other metals, including toxic species, in the near surface environment, especially because these micas are abundant in many rocks and soils.

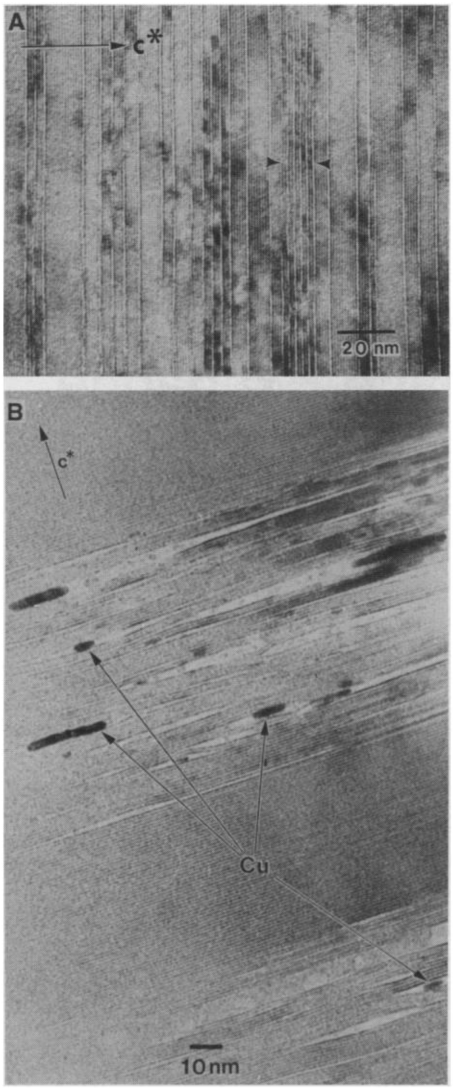

Fig. 8. (**A**) Partially vermiculitized region of a natural Cu-bearing biotite (dark fringes correspond to the individual mica layers). Detectable Cu is restricted to areas such as this that show expanded interlayers, and analyses of this region indicate $\sim$3.5% CuO by weight. Arrowheads point out several layers with hydrobiotite (alternating vermiculite-mica) ordering (*64*). (**B**) HRTEM image of a biotite crystal that was experimentally reacted with an acidic $CuSO_4$ solution at 25°C (*65*). Small crystals of metallic Cu are indicated (*65*). [Modified from (*64, 65*)]

The imaging, diffraction, and analytical capabilities of the TEM are complemented by other modern analytical methods, especially surface analytical techniques such as Auger electron spectroscopy or x-ray photoelectron spectroscopy (XPS) (*12, 66*). The combination of TEM and XPS has been used to demonstrate that Fe^{2+} in mica can reduce Ag^+ from solution in rapid, vigorous surface and internal reactions (*67*). The relatively toxic, soluble species Cr^{6+}, however, is reduced and efficiently bound to the biotite surface as a less soluble Cr^{3+} species. This redox reaction shows strong crystallographic specificity, occurring much more rapidly on the (*hk*0) crystal edges than on the basal (001) cleavage faces. Although compositional sector zoning occurs during growth of many rock-forming minerals, such dramatic effects of crystallographic orientation on kinetics of surface reactions have not been commonly recognized in silicates.

Future Directions in TEM of Minerals

As suggested by some of the above examples, most Earth processes leave a mineralogical record consisting of physical or chemical heterogeneities, and many of these heterogeneities are beyond the resolution of conventional light microscopes. These processes include (i) crystallization from other solids, a silicate melt, or an aqueous fluid; (ii) deformation of minerals and rocks; (iii) phase separation resulting from immiscibility during cooling of a mineral; (iv) phase transitions that result from changes in temperature and pressure; and (v) chemical reactions occurring during metamorphism, hydrothermal alteration, or weathering. These processes in many ways are analogous to those studied by materials scientists, solid-state physicists, and solid-state chemists.

Parallels between the applications of TEM methods in the materials sciences and those in the geochemical and geophysical sciences are common. Indeed, early materials microscopists studied simple metals and alloys, and early mineralogical applications of HRTEM largely involved well-crystallized and museum-quality specimens of simple minerals [for example (*68*)]. Geological applications are rapidly becoming more process-oriented, similar to many materials investigations. Just as investigators working with synthetic solids have turned to sophisticated combinations of approaches, such as TEM combined with surface analytical techniques and synchrotron x-ray diffraction and spectroscopy, Earth scientists are also making use of a wider array of experimental methods. For example, one of the frontiers is to understand at the atomic level the complex interplay among aqueous fluid chemistry, chemical reactions that take place in minerals, and surface reactions. Such fluid-mineral interactions play a key role in petrogenesis under diverse conditions, ranging from surficial weathering to hydrothermal reactions in Earth's upper mantle. Conversely, Earth scientists are increasingly turning to TEM observations on synthetic systems. For example, complete mechanistic understanding of reactions that take place within the high-pressure diamond anvil cell requires not only in situ observations by optical microscopy, Raman spectroscopy, and synchrotron x-ray diffraction, but also characterization of the final experimental products with TEM (*69*).

REFERENCES AND NOTES

1. A. Navrotsky and D. J. Weidner, Eds., *Perovskite: A Structure of Great Interest to Geophysics and Materials Science* (American Geophysical Union, Washington, DC, 1989); M. Hu, H.-R. Wenk, D. Sinitsyna, *Am. Mineral.* **77**, 359 (1992).
2. B. Raveau, C. Michel, M. Hervieu, D. Groult, J. Provost, *J. Solid State Chem.* **85**, 181 (1990).
3. P. Hirsch, A. Howie, R. B. Nicholson, D. W. Pashley, M. J. Whelan, *Electron Microscopy of Thin Crystals* (Krieger, Melbourne, FL, ed. 2, 1977).
4. H.-R. Wenk *et al.*, Eds., *Electron Microscopy in Mineralogy* (Springer-Verlag, Berlin, 1976).
5. H. W. Green, II, in *Minerals and Reactions at the Atomic Scale: Transmission Electron Microscopy*, P. R. Buseck, Ed. (*Rev. Mineral.* **27**, Mineralogical Society of America, Washington, DC, 1992), pp. 425–454.
6. G. L. Nord, Jr., in *ibid.*, pp. 455–508.
7. J. I. Goldstein, D. B. Williams, G. Cliff, in *Principles of Analytical Electron Microscopy*, D. C. Joy, A. D. Romig, Jr., J. I. Goldstein, Eds. (Plenum, New York, 1986), pp. 155–217.
8. J. W. Steeds and J.-P. Morniroli, in *ibid.*, pp. 37–84; J. C. H. Spence and J. M. Zuo, *Electron Microdiffraction* (Plenum, New York, 1992).
9. P. R. Buseck, J. M. Cowley, L. Eyring, Eds., *High-Resolution Transmission Electron Microscopy* (Oxford Univ. Press, New York, 1988); D. C. Joy, A. D. Romig, Jr., J. I. Goldstein, Eds., *Principles of Analytical Electron Microscopy* (Plenum, New York, 1986).
10. F. C. Hawthorne, Ed., *Spectroscopic Methods in Mineralogy and Geology* (*Rev. Mineral.* **18**, Mineralogical Society of America, Washington, DC, 1988).
11. J. F. Stebbins and I. Farnan, *Science* **245**, 257 (1989).
12. M. F. Hochella, Jr., in (*10*), pp. 573–637.
13. P. K. Hansma, V. B. Elings, O. Marti, C. E. Bracker, *Science* **242**, 209 (1988).
14. S. R. Bohlen and D. H. Lindsley, *Annu. Rev. Earth Planet. Sci.* **15**, 397 (1987).
15. A. C. Lasaga, S. M. Richardson, H. D. Holland, in *Energetics of Geological Processes*, S. K. Saxena and S. Bhattacharji, Eds. (Springer-Verlag, New York, 1977), pp. 353–388.
16. J. F. Banfield, D. R. Veblen, D. J. Smith, *Am. Mineral.* **76**, 343 (1991).
17. R. Marchand, L. Brohan, M. Tournoux, *Mater. Res. Bull.* **15**, 1129 (1980).
18. K. H. Downing, H. Meisheng, H.-R. Wenk, M. A. O'Keefe, *Nature* **348**, 525 (1990).
19. M. Amouric and A. Baronnet, *Phys. Chem. Miner.* **9**, 146 (1983); A. Meike, H.-R. Wenk, M. A. O'Keefe, R. Gronsky, *ibid.* **15**, 427 (1988); D. R. Peacor, in (*5*), pp. 335–380; R. J. Reeder, in (*5*), pp. 381–424.

20. At different temperatures, for example, synthetic rutile accommodates nonstoichiometry through different types of defects, including vacancies, crystallographic shear planes, and planar features known as platelet defects: M. G. Blanchin, L. A. Bursill, D. J. Smith, *Proc. R. Soc. London Ser. A* **391**, 351 (1984); L. A. Bursill, M. G. Blanchin, D. J. Smith, *ibid.*, p. 373.
21. Similarly, ion-exchange reactions between minerals may occur by transport through the intergranular medium, which is commonly an aqueous fluid in crustal rocks [D. M. Carmichael, *Contrib. Mineral. Petrol.* **20**, 244 (1969)]. In such reactions, dislocations and other defects may influence the kinetics of dissolution and precipitation, but they do not appear to interact structurally in the reaction mechanism [A. Baronnet, *Fortschr. Mineral.* **62**, 187 (1984)]. We therefore do not consider such dissolution-precipitation reactions further.
22. Following the usage of H. Schmalzried [*Solid State Reactions* (Verlag Chemie, Weinheim, 1981)], a reaction is solid-state if it involves solid reactants and products, even if a fluid phase is involved also as a catalyst.
23. D. R. Veblen and P. R. Buseck, *Am. Mineral.* **65**, 599 (1980).
24. J. B. Brady and R. H. McCallister, *ibid.*, **68**, 95 (1983).
25. D. R. Veblen, *ibid.* **76**, 801 (1991).
26. R. J. Angel, *ibid.* **71**, 1441 (1986); J. F. Banfield and R. A. Eggleton, *Clays Clay Minerals* **36**, 47 (1988); J. F. Banfield, D. R. Veblen, B. F. Jones, *Contrib. Mineral. Petrol.* **106**, 110 (1990).
27. S. Iijima, *J. Solid State Chem.* **14**, 52.
28. R. J. D. Tilley, *Defect Crystal Chemistry and Its Applications* (Blackie, Glasgow, 1987).
29. J. W. Christian, *The Theory of Transformations in Metals and Alloys, Part I: Equilibrium and General Kinetic Theory* (Pergamon, Oxford, ed. 2, 1975).
30. P. W. McMillan, *Glass-Ceramics* (Academic Press, New York, ed. 2, 1979).
31. G. L. Nord, Jr., A. H. Heuer, J. S. Lally, in (*4*), pp. 220–227.
32. C. Willaime, W. L. Brown, M. Gandais, in (*4*), pp. 248–257; T. L. Grove, *Contrib. Mineral. Petrol.* **64**, 273 (1977).
33. For review, see R. A. Yund, in *Feldspar Mineralogy*, P. H. Ribbe, Ed. (*Rev. Mineral.* **2**, Mineralogical Society of America, Washington, DC, ed. 2, 1983), pp. 177–202.
34. K. J. T. Livi and D. R. Veblen, *Am. Mineral.* **74**, 1070 (1989).
35. P. Robinson, M. Ross, G. L. Nord, Jr., J. R. Smyth, H. W. Jaffe, *ibid.* **62**, 857 (1977); K. J. T. Livi, *Contrib. Mineral. Petrol.* **96**, 371 (1987).
36. M. Ross, J. J. Papike, K. W. Shaw, *Mineral. Soc. Am. Spec. Pap.* **2**, 275 (1969); for review, see P. Robinson *et al.*, in *Amphiboles—Petrology and Experimental Phase Relations*, D. R. Veblen and P. H. Ribbe, Eds. (*Rev. Mineral.* **9B**, Mineralogical Society of America, Washington, DC, 1982), pp. 1–227.
37. E. A. Smelik and D. R. Veblen, *Science* **257**, 1669 (1992).
38. E. A. Smelik, M. W. Nyman, D. R. Veblen, *Am. Mineral.* **76**, 1184 (1991); E. A. Smelik and D. R. Veblen, *ibid.* **78**, 511 (1993).
39. Y.-H. Shau, D. R. Peacor, S. Ghose, P. P. Phakey, *ibid.* **78**, 96 (1993).
40. Amphiboles are classified according to the occupancy of the *M4* crystallographic site as ferromagnesian (*M4* = Fe, Mg, and Mn), sodic (*M4* = Na), calcic (*M4* = Ca), or sodic-calcic (*M4* = Na and Ca) [B. E. Leake, *ibid.* **63**, 1023 (1978)].
41. E. A. Smelik and D. R. Veblen, *ibid.* **76**, 971 (1991); *Contrib. Mineral. Petrol.* **112**, 178 (1992).
42. J. Laird and A. L. Albee, *Am. J. Sci.* **281**, 127 (1981).
43. E. A. Smelik and D. R. Veblen, in preparation.
44. Compositions of fluids in inclusions are commonly estimated from freezing and homogenization temperatures obtained with light microscopes [E. Roedder, *Fluid Inclusions* (*Rev. Mineral.* **12**, Mineralogical Society of America, Washington, DC, 1984)].
45. O. Navon, I. D. Hutcheon, G. R. Rossman, G. J. Wasserburg, *Nature* **335**, 784 (1988).
46. G. D. Guthrie, Jr., D. R. Veblen, O. Navon, G. R. Rossman, *Earth Planet. Sci. Lett.* **105**, 1 (1991).
47. G. D. Guthrie, Jr., and D. R. Veblen, *Contrib. Mineral. Petrol.* **108**, 298 (1992).
48. K. Yagi, in *High-Resolution Transmission Electron Microscopy*, P. R. Buseck, J. M. Cowley, L. Eyring, Eds. (Oxford Univ. Press, New York, 1988), pp. 568–606.
49. G. Van Tendeloo *et al.*, *Phase Transitions* **27**, 61 (1990); A. N. Goldstein, C. M. Echer, A. P. Alivisatos, *Science* **256**, 1425 (1992).
50. N. Shimobayashi, *Am. Mineral.* **77**, 107 (1992).
51. S. Ghose, G. Van Tendeloo, S. Amelinckx, *Science* **242**, 1539 (1988).
52. For reviews, see G. Dolino, *Phase Transitions* **21**, 59 (1990); P. J. Heaney and D. R. Veblen, *Am. Mineral.* **76**, 1018 (1991).
53. G. Van Tendeloo, J. Van Landuyt, S. Amelinckx, *Phys. Status Solidi* **33**, 723 (1976).
54. G. Dolino, J. P. Bachheimer, B. Berge, C. M. E. Zeyen, *J. Phys.* **45**, 361 (1984).
55. J. D. C. McConnell, *Am. Mineral.* **68**, 1 (1983); H. Böhm, *ibid.*, p. 11; J. M. Cowley, J. B. Cohen, M. B. Salamon, B. J. Wuensch, Ed., *Modulated Structures—1979* (American Institute of Physics, New York, 1979).
56. J. P. Jamet, *Phase Transitions* **11**, 335 (1988).
57. I. Hatta, M. Matsuura, H. Yao, K. Gouhara, N. Kato, *Thermochim. Acta* **88**, 143 (1985).
58. G. Dolino, F. Mogeon, P. Bastie, *Phys. Status Solidi A* **107**, 559 (1988).
59. P. Lederer, G. Montambaux, J. P. Jamet, M. Chauvin, *J. Phys. Lett.* **45**, L627 (1984).
60. P. J. Heaney and D. R. Veblen, *Am. Mineral.* **76**, 1459 (1991).
61. P. R. Buseck and D. R. Veblen, *Geochim. Cosmochim. Acta* **42**, 669 (1978).
62. J. J. Papike, in *Pyroxenes*, C. T. Prewitt, Ed. (*Rev. Mineral.* **7**, Mineralogical Society of America, Washington, DC, 1980), pp. 495–525.
63. G. E. Harlow and D. R. Veblen, *Science* **251**, 652 (1991).
64. E. S. Ilton and D. R. Veblen, *Nature* **334**, 516 (1988); *Econ. Geol.*, in press.
65. E. S. Ilton, D. Earley, III, D. Morozas, D. R. Veblen, *ibid.*, **87**, 1813 (1992).
66. B. M. Bakken, M. F. Hochella, Jr., A. F. Marshall, A. M. Turner, *ibid.* **84**, 171 (1989).
67. E. S. Ilton and D. R. Veblen, in preparation.
68. P. R. Buseck and S. Iijima, *Am. Mineral.* **59**, 1 (1974).
69. K. J. Kingma, C. Meade, R. J. Hemley, H.-k. Mao, D. R. Veblen, *Science* **259**, 666 (1993).
70. Most of the work presented here was done while the authors were in the Department of Earth and Planetary Sciences, Johns Hopkins University. The research was first presented in this form as the inaugural Gabriella Donnay Lecture at the Carnegie Institution of Washington Geophysical Laboratory. G. Donnay and J. D. H. Donnay were among the first x-ray crystallographers to comprehend the power of HRTEM for solving crystallographic problems and this article is warmly dedicated to them. We thank D. J. Smith for collaboration in the study of TiO_2. The research was funded by the National Science Foundation and the Department of Energy.

Atmosphere-Surface Exchange Measurements

W. F. Dabberdt, D. H. Lenschow, T. W. Horst, P. R. Zimmerman, S. P. Oncley, A. C. Delany

The exchange of various trace species and energy at the earth's surface plays an important role in climate, ecology, and human health and welfare. Surface exchange measurements can be difficult to obtain yet are important to understand physical processes, assess environmental and global change impacts, and develop robust parameterizations of atmospheric processes. The physics and turbulent structure of the atmospheric boundary layer are reviewed as they contribute to dry surface exchange rates (fluxes). Micrometeorological, budget, and enclosure techniques used to measure or estimate surface fluxes are described, along with their respective advantages and limitations. Various measurement issues (such as site characteristics, sampling considerations, sensor attributes, and flow distortion) impact on the ability to obtain representative surface-based and airborne flux data.

There is widespread concern about the effect of anthropogenic activities on the composition of the earth's atmosphere. A major limitation in our understanding of the chemistry of the atmosphere is uncertainty over the distribution and rates of change of trace species emissions and losses at the earth's surface. Although small and difficult to quantify accurately on the local scale, these exchanges nonetheless are very significant when integrated over the larger scales. For example, distributed emissions from rural lands and oceans are as important as locally intense industrial emissions.

Surface exchange studies range in scale from investigations of specific microbial biochemistry to projections of changes in the composition of the global atmosphere. Trace gases are both emitted and absorbed at the earth's surface. The resulting fluxes are of great importance in studying the budgets of trace species—that is, their sources, sinks, transformations, and transport. These processes interact across a broad spectrum of temporal and spatial scales. Thus, for example, investigations of soil nutrient cycling (and its dependence on

---

The authors are with the National Center for Atmospheric Research, P.O. Box 3000, Boulder, CO 80307–3000.